Eur. J. Mineral.
2018, **30**, 621–634
Published online 27 April 2018

Crystal chemistry of schoonerite-group minerals

Ian Edward GREY[1,*], Anthony R. KAMPF[2], Erich KECK[3], Colin M. MacRAE[1], John D. CASHION[4] and Yesim GOZUKARA[5]

[1] CSIRO Mineral Resources, Private Bag10, Clayton, Victoria, 3169, Australia
*Corresponding author, e-mail: ian.grey@csiro.au
[2] Mineral Sciences department, Natural History Museum of Los Angeles County, 900 Exposition Boulevard, Los Angeles, California 900007, USA
[3] Algunderweg 3, 92694 Etzenricht, Germany
[4] Monash University, School of Physics and Astronomy, Victoria 3800, Australia
[5] CSIRO Manufacturing, Private Bag 10, Clayton South, Victoria 3169, Australia

Abstract: Synchrotron single-crystal structure refinements for five schoonerite-group minerals (SGMs) from the Hagendorf Süd, Bavaria, and Palermo No.1, New Hampshire, pegmatites were combined with results from previous studies on type schoonerite and the SGMs wilhelmgümbelite and schmidite to evaluate the main crystallochemical relations between the minerals. Elements Zn and Fe^{3+} are essential to the structure and are ordered in specific sites, while Mn and Fe are distributed relatively uniformly over three octahedral sites, *M*1, *M*2 and *M*3. The Mn/(Mn + Fe) atomic ratio is relatively constant for the samples studied, ~0.26–0.31, and is close to this ratio in the primary phosphate, triphylite, from which the SGMs are derived. The main crystallochemical variations are due to different degrees of oxidation of the Fe, which ranges from 45% of the total Fe as Fe^{3+} in green SGMs, to 98% of the Fe as Fe^{3+} in red SGMs. The Fe oxidation state is linked to a significant structural change, whereby Zn in a trigonal bipyramidal site, $^{[5]}$Zn, is partially partitioned into an adjacent tetrahedral site, $^{[4]}$Zn, when the amount of Fe as Fe^{3+} increases above 70% There is an apparent correlation between the extent of partitioning of Zn, and cation deficiency in the *M*3 site, leading to a general formula for SGMs: $[^{[4]}(Zn,Fe)_x\ ^{[5]}(Zn,Fe)_{1-x}]$ *M*1 *M*2 $(M3_{1-x}\square_x)$ $Fe^{3+}(PO_4)_3(OH)_y(H_2O)_{9-y}\cdot 2H_2O$; where □ = vacancy and $x \leq 0.3$. The sites *M*1, *M*2 and *M*3 contain varying amounts of Fe^{2+}, Fe^{3+}, Mn^{2+} and Zn, with minor Mg. The different SGMs are distinguished by the dominant-cations and their oxidation states in the *M*1, *M*2 and *M*3 sites. Wilhelmgümbelite has $M1 = Fe^{3+}$, $M2 = Fe^{3+}$, $M3 = Fe^{2+}$, while schmidite has $M1 = (Fe^{3+}_{0.5}Mn^{2+}_{0.5})$, $M2 = (Fe^{3+}_{0.5}Mn^{2+}_{0.5})$, $M3 = Zn$ and schoonerite has $M1 = Mn^{2+}$, $M2 = Fe^{2+}$, $M3 = Fe^{2+}$. One of the SGMs studied was found to have a new ordering of dominant-cations of dominant-valency, with $M1 = (Fe^{3+}_{0.5}Mn^{2+}_{0.5})$, $M2 = (Fe^{3+}_{0.5}Mn^{2+}_{0.5})$, $M3 = Mn^{2+}$, and it has subsequently been approved as the new mineral wildenauerite (IMA 2017-058).

Key-words: schoonerite; schmidite; wilhelmgümbelite; wildenauerite; Hagendorf Süd pegmatite; Palermo No.1 pegmatite; crystal structure; Mössbauer spectroscopy.

1. Introduction

Schoonerite, $ZnMnFe^{2+}_2Fe^{3+}(PO_4)_3(OH)_2(H_2O)_7\cdot 2H_2O$, was first described as a new species from the Palermo No. 1 pegmatite, New Hampshire, by Moore & Kampf (1977). The type specimen was found in a corroded triphylite pod in which the triphylite had been replaced by siderite and the hydrated Fe^{2+}-containing phosphate minerals ludlamite, messelite and vivianite. Brown to copper-red schoonerite laths and other oxidized secondary phosphates were perched on the earlier-formed Fe^{2+}-containing minerals. The essential Zn in schoonerite was considered to derive from sphalerite, which is a common constituent of the phosphate pods.

Kampf (1977) determined the structure of schoonerite and noted its structural relationship to montgomeryite, olmsteadite and melonjosephite. Schoonerite is orthorhombic, with $a = 11.12$, $b = 25.55$ and $c = 6.44$ Å; the structure was solved in space group *Pmab*, an alternative setting of *Pbcm*. It has a complex layer structure, illustrated in Fig. 1, in which 6.4 Å chains of edge-sharing *M*2- and *M*3-centred octahedra (normal to the figure) containing Fe^{2+} are linked along [100] by corner-sharing to 6.4 Å chains comprising alternating corner-linked $P2O_4$ tetrahedra and *M*4-centred octahedra ($M4 = Fe^{3+}$). Five-coordinated Zn polyhedra, $^{[5]}$Zn, share an edge with the $P2O_4$ tetrahedra. A second phosphate group, $P1O_4$, cross-links the *M*2- and *M*4-centred octahedra with $^{[5]}$Zn, and with isolated *M*1-centred octahedra containing Mn^{2+}, forming {010} slabs as shown in Fig. 1. Water molecules are located between the {010} heteropolyhedral slabs and hydrogen bond to oxygen atoms at the surface of the slabs.

Downloaded from https://pubs.geoscienceworld.org/eurjmin/article-pdf/30/3/621/4346636/ejm_30_3_0621_0634_grey_2707_online.pdf
by University of Arizona user
on 27 September 2018

https://dx.doi.org/10.1127/ejm/2018/0030-2707
0935-1221/18/0030-2707 $ 6.30

© 2018 E. Schweizerbart'sche Verlagsbuchhandlung, D-70176 Stuttgart

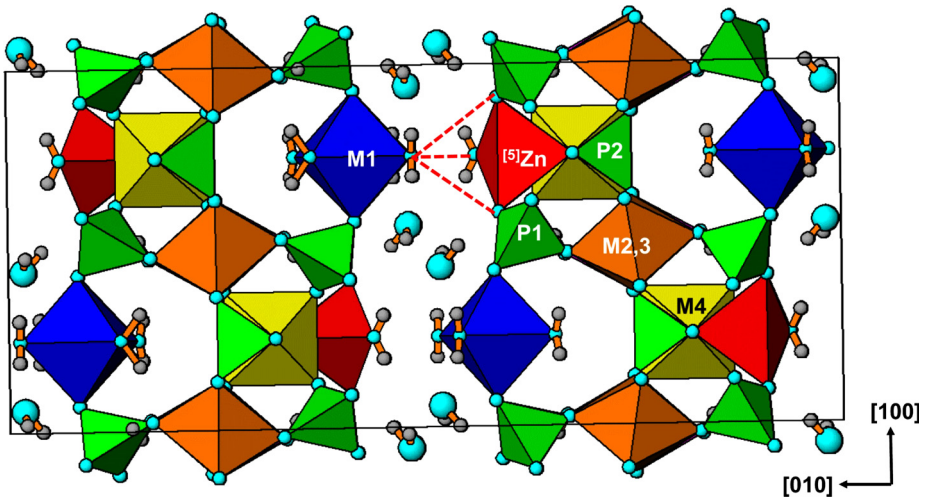

Fig. 1. [001] Projection of the schoonerite structure. The outline of the $^{[4]}$Zn tetrahedron is shown by the dashed lines.

We have recently characterized two new schoonerite group minerals (SGMs) from the Hagendorf Süd granitic pegmatite in Bavaria. They are wilhelmgümbelite, $ZnFe^{2+}Fe_3^{3+}(PO_4)_3(OH)_4(H_2O)_5{\cdot}2H_2O$ (IMA2015-072; Grey *et al.*, 2017a) and schmidite, $Zn_2(Fe_{0.5}^{3+},Mn_{0.5}^{2+})_2Fe^{3+}(PO_4)_3(OH)_3(H_2O)_6{\cdot}2H_2O$ (IMA2017-012; Grey *et al.*, 2017b). In contrast to schoonerite, both minerals have Fe predominantly as Fe^{3+} and have the Zn partitioned between the $^{[5]}$Zn site and an adjacent tetrahedrally coordinated site, $^{[4]}$Zn, separated from $^{[5]}$Zn by ~1 Å. Crystal structure refinements combined with analytical data revealed that dominant Zn in $^{[5]}$Zn/$^{[4]}$Zn and dominant Fe^{3+} in *M*4 are consistent crystallochemical features of SGMs, but significant differences occur in the occupation of the *M*1, *M*2 and *M*3 sites. The SGMs are distinguished by the dominant cations and their oxidation states (Hatert & Burke, 2008) in these three sites. Schoonerite is reported to have $M1 = Mn^{2+}$, $M2 = Fe^{2+}$, $M3 = Fe^{2+}$ (Kampf, 1977), wilhelmgümbelite has $M1 = Fe^{3+}$, $M2 = Fe^{3+}$, $M3 = Fe^{2+}$ (Grey *et al.*, 2017a), and schmidite has $M1 = (Fe_{0.5}^{3+}Mn_{0.5}^{2+})$, $M2 = (Fe_{0.5}^{3+}Mn_{0.5}^{2+})$, $M3 = Zn$ (Grey *et al.*, 2017b). The schoonerite group has been approved by the IMA Commission for New Minerals, Naming and Classification (Grey *et al.*, 2017c).

In view of the significant crystallochemical differences between schoonerite and the oxidized SGM minerals, wilhelmgümbelite and schmidite, we undertook a more extensive study of SGMs, covering a range of Fe^{2+}/Fe^{3+}, in minerals from both the Hagendorf Süd and the Palermo No.1 pegmatites, to determine the influence of Fe oxidation state on the crystal chemistry. We describe here the application of synchrotron single-crystal structure refinements, Mössbauer spectroscopy, electron microprobe analyses (EMPA) and thermal analyses to elucidate the crystallochemical changes associated with variations in the iron oxidation state, as well as in the Mn/Fe/Zn contents.

Fig. 2. Clusters of green brown SGM crystals in vug on right hand side, and orange red SGM crystals in specimen from the Palermo No.1 pegmatite. Field of view 7 mm.

2. Experimental procedure

2.1. Samples

The two Palermo samples were taken from the same micromount specimen in the collection of the Natural History Museum of Los Angeles County. A photomicrograph of the crystals is shown in Fig. 2. The greenish-brown crystals (henceforth designated Palermo brown) form radiating sprays in a small vug on the right-hand side, while sprays of orange-red crystals (Palermo red) are scattered over the left-hand part of the figure. The main matrix mineral is siderite, and other associated minerals include large, colourless, blocky crystals of whitlockite coated with mitridatite, and orange, equant crystals of laueite.

The SGM-bearing samples IGC-2, IGC-11, IGC-14 and IGC-65 were collected by one of us (E.K.) from the mine at Hagendorf Süd, Bavaria, in the 1970s. Samples IGC-11 and IGC-14 were collected from 60 to 67 m level in the

Downloaded from https://pubs.geoscienceworld.org/eurjmin/article-pdf/30/3/621/4346636/ejm_30_3_0621_0634_grey_2707_online.pdf
by University of Arizona user
on 27 September 2018

Table 1. Analytical data (wt%) for schoonerite group minerals. Standard deviation in parentheses.

	Hagendorf Süd IGC-65	Hagendorf Süd IGC-14	Palermo red	Palermo brown	Hagendorf Süd IGC-2	Hagendorf Süd IGC-11	Probe standard
No. of Analyses	6	10	7	9	9	10	
MnO	8.8(1.2)	10.7(7)	8.6(2)	8.8(4)	11.0(8)	10.9(5)	Rhodonite
ZnO	13.5(6)	11.5(7)	12.8(1.0)	12.9(2)	13.9(6)	9.8(8)	Phosphophyllite
MgO	0.22(7)	0.28(8)	0.65(7)	0.7(1)	0.3(1)	0.25(5)	Spinel
FeO*	0.2	0.7	2.6	7.8	7.4	15.0	
Fe_2O_3	26.6	25.2	23.0	16.9	17.5	13.6	Hematite
P_2O_5	27.6(3)	27.2(4)	27.9(9)	27.3(8)	29.0(3)	28.6(4)	Berlinite
H_2O**	22.2	24.5	23.3	23.4	23.5	23.9	
Total	100.4	100.1	98.8	97.8	102.6	102.0	
Empirical formulae							ΣM
IGC-65	$Zn_{1.26}Mn^{2+}_{0.91}Mg_{0.04}Fe^{2+}_{0.03}Fe^{3+}_{2.60}(PO_4)_3(OH)_{3.28}(H_2O)_{7.72}$						4.84
IGC-14	$Zn_{1.11}Mn^{2+}_{1.18}Mg_{0.05}Fe^{2+}_{0.08}Fe^{3+}_{2.47}(PO_4)_3(OH)_{3.25}(H_2O)_{7.75}$						4.87
Palermo red	$Zn_{1.20}Mn^{2+}_{0.93}Mg_{0.12}Fe^{2+}_{0.25}Fe^{3+}_{2.21}(PO_4)_3(OH)_{2.63}(H_2O)_{8.37}$						4.71
Palermo brown	$Zn_{1.23}Mn^{2+}_{0.96}Mg_{0.13}Fe^{2+}_{0.85}Fe^{3+}_{1.65}(PO_4)_3(OH)_{2.29}(H_2O)_{8.71}$						4.82
IGC-2	$Zn_{1.25}Mn^{2+}_{1.14}Mg_{0.06}Fe^{2+}_{0.76}Fe^{3+}_{1.60}(PO_4)_3(OH)_{2.22}(H_2O)_{8.78}$						4.81
IGC-11	$Zn_{0.90}Mn^{2+}_{1.15}Mg_{0.05}Fe^{2+}_{1.58}Fe^{3+}_{1.26}(PO_4)_3(OH)_{2.14}(H_2O)_{8.86}$						4.94

* Proportion of iron as FeO from Mössbauer for Hagendorf Süd samples and from <*M*−O> *vs. a* cell parameter for Palermo samples.
** From thermal analysis for IGC-11 and IGC-14, and from structure and charge balance for other samples.

Fig. 3. Banded sequence of radial rockbridgeite (dark grey) and schoonerite-group minerals (orange red) from Hagendorf Süd. Photo by Volker Betz, Field of view ~3 cm.

mine, IGC-65 from 67 to 70 m, and sample IGC-2 from a depth of 76 m. In all specimens, the SGM crystals are in close association with rockbridgeite and jahnsite. The SGM and rockbridgeite form alternating bands of dense lamellae, illustrated in Fig. 3. The colour of the SGM crystals varies from green to brown to red, often over distances of a few mm. In sample IGC-2, dense hemispherical mounds of brownish-green radially distributed crystals were observed. In sample IGC-65, the SGM forms crusts of corroded orange crystals, intimately mixed with jahnsite and rockbridgeite. Other associated minerals in the hand specimens include vivianite, apatite and strunzite. The close association of SGMs with rockbridgeite in the four Hagendorf Süd samples contrasts with the association of wilhelmgümbelite and schmidite with phosphophyllite (and vivianite in the case of schmidite).

2.2. Analyses

Crystals of all specimens were analysed using wavelength dispersive spectrometry on a JEOL JXA 8500F Hyperprobe operated at an accelerating voltage of 15 kV and a beam current of 4 nA. The beam was defocused to 2 μm. Analytical results are given in Table 1. EMPA results for associated rockbridgeite and jahnsite are reported in Table 2.

Laser induced breakdown spectroscopy (LIBS) was used to determine Li contents. The analyses were done on pressed powders and the results averaged from 30 point analyses (3 lines of 10 points) and compared to OPEG Li pressed powder standards.

2.3. Mössbauer spectroscopy

Pure SGMs were separated from samples IGC-2, IGC-11 and IGC-14 under a binocular microscope, and the phase purity was confirmed from powder X-ray diffraction (PXRD) scans. Mössbauer spectra of the pure specimens were taken using a conventional constant acceleration drive with a symmetrical sawtooth waveform (Wissel). The source of ^{57}Co in rhodium was maintained at room temperature. The spectra were fitted using Voigtian doublets comprising a Lorentzian half width at half maximum (HWHM) component of typically 0.14 mm/s and a variable Gaussian component to deal with line broadening. The results for isomer shifts δ, quadrupole splitting Δ, Gaussian component $\sigma(\Delta)$ and doublet relative areas are reported in Table 3, together with assignments. The isomer shifts are given relative to α-Fe at room temperature. The fitted spectrum for the SGM in sample IGC-2 is shown in Fig. 4.

Downloaded from https://pubs.geoscienceworld.org/eurjmin/article-pdf/30/3/621/4346636/ejm_30_3_0621_0634_grey_2707_online.pdf
by University of Arizona user
on 27 September 2018

Table 2. Analytical data (wt%) for minerals associated with Hagendorf Süd schoonerite group minerals. Standard deviation in parentheses.

	IGC-65 Rockbridgeite	IGC-65 Jahnsite-(CaMnFe)	IGC-14 Rockbridgeite	IGC-14 Jahnsite-(CaMnFe)	IGC-11 Rockbridgeite	IGC-2 Jahnsite-(CaMnFe)
No. of analyses	3	8	9	10	11	11
MnO	4.2(2)	12.8(4)	5.3(3)	14.7(7)	5.3(2)	13.9(5)
ZnO	4.6(3)	4.0(1.8)	4.5(8)	1.6(4)	2.9(4)	2.6(7)
MgO	0.05(1)	0.59(9)	0.01(4)	0.77(9)	0.03(5)	0.87(8)
CaO	0.3(1)	3.7(1.5)	0.5(1)	4.5(6)	0.6(1)	4.3(4)
Fe_2O_3[a]	50.7(2)	26.3(1.0)	47.6(1.3)	26.7(1.1)	53.0(1.1)	25.0(1.5)
Al_2O_3	0.6(2)	0.2(2)	0.01(3)	0.05(5)	0.01(3)	0.9(8)
P_2O_5	32.5(1.0)	31.2(7)	31.8(3)	31.6(4)	33.3(4)	32.9(5)
H_2O[b]	6.5	19.0	7.2	18.6	6.8	19.6
Total	99.4	97.8	96.9	98.5	101.4	100.1
Empirical formulae, normalised to 4 P and 26 anions for jahnsite and to 3 P and 17 anions for rockbridgeite						
Jahnsite in IGC-65	$Ca_{0.60}Mn^{2+}_{1.60}Zn_{0.45}Mg_{0.13}Fe^{2+}_{1.03}Fe^{3+}_{1.97}Al_{0.03}(PO_4)_4(OH)_{1.62}(H_2O)_{8.38}$					
Jahnsite in IGC-14	$Ca_{0.72}Mn^{2+}_{1.86}Zn_{0.18}Mg_{0.17}Fe^{2+}_{1.02}Fe^{3+}_{2.00}(PO_4)_4(OH)_{1.90}(H_2O)_{8.10}$					
Jahnsite in IGC-2	$Ca_{0.66}Mn^{2+}_{1.69}Zn_{0.28}Mg_{0.93}Fe^{2+}_{0.85}Fe^{3+}_{1.85}Al_{0.15}(PO_4)_4(OH)_{1.34}(H_2O)_{8.66}$					
Rockbridgeite in IGC-65[c]	$Ca_{0.04}Mn^{2+}_{0.39}Zn_{0.37}Fe^{3+}_{4.16}Al_{0.08}(PO_4)_3O_{0.32}(OH)_{4.68}$					
Rockbridgeite in IGC-14	$Ca_{0.06}Mn^{2+}_{0.50}Zn_{0.37}Fe^{3+}_{3.99}(PO_4)_3(OH)_{4.83}(H_2O)_{0.17}$					
Rockbridgeite in IGC-11	$Ca_{0.07}Mn^{2+}_{0.48}Zn_{0.23}Fe^{3+}_{4.24}(PO_4)_3O_{0.28}(OH)_{4.72}$					

[a] Total Fe as Fe_2O_3.
[b] from mineral formulae.
[c] Unknown Fe^{2+} contribution in rockbridgeite minerals.

Table 3. ^{57}Fe Mössbauer parameters for schoonerite group minerals.

	Red schoonerite IGC-14				Brown green schoonerite IGC-2				Green schoonerite IGC-11				Assignment
	δ mm/s	Δ mm/s	σ(Δ)	*A*(%)	δ mm/s	Δ mm/s	σ(Δ)	*A*(%)	δ mm/s	Δ mm/s	σ(Δ)	*A*(%)	
Fe^{3+}	0.39(1)	0.50(9)	0.13(7)	47	0.44(1)	0.49(1)	0.11(3)	40	0.38(1)	0.44(1)	0.10(2)	45	Fe4
Fe^{3+}	0.39(1)	0.86(15)	0.17(20)	38	0.40(1)	1.13(13)	0.42(9)	28					Fe1 + Fe2
Fe^{3+}	0.38(2)	1.3(6)	0.24(25)	12									Fe3
Fe^{2+}					1.30(5)	1.4(3)	0.2(1)	6	1.37(1)	1.03(3)	0.08(6)	7	
Fe^{2+}					1.27(5)	2.0(2)	0.1(5)	3	1.23(2)	1.61(6)	0.0(6)	3	
Fe^{2+}					1.22(3)	2.48(6)	0.0(3)	10	1.15(1)	2.43(1)	0.06(1)	39	
Fe^{2+}	0.96(9)	2.65(17)	0.43(18)	3	1.34(5)	2.65(9)	0.1(1)	13					

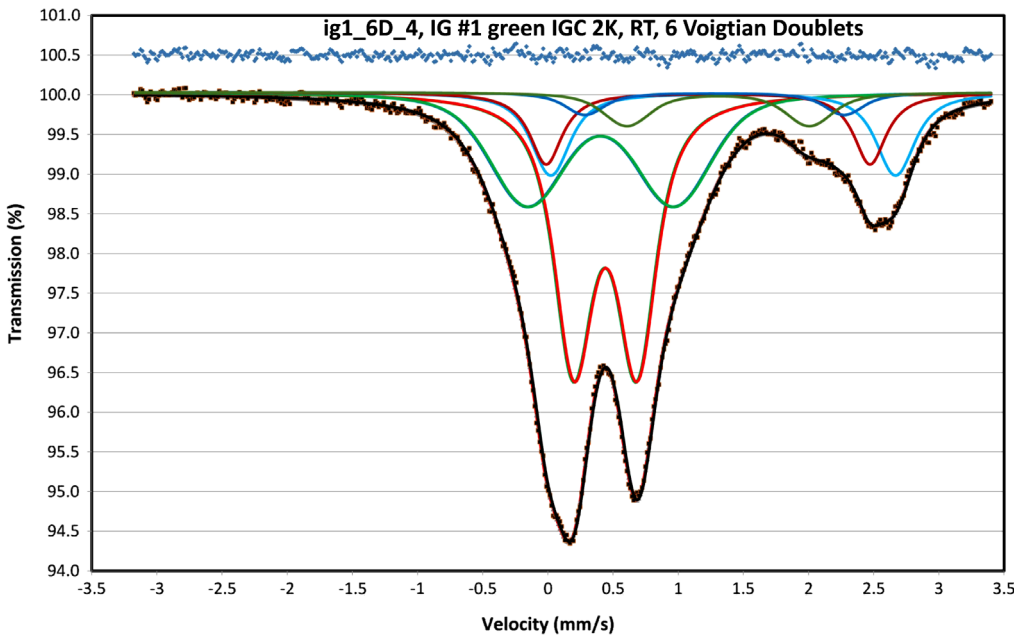

Fig. 4. Fitted Mössbauer spectrum for brown green SGM, sample IGC-2, from Hagendorf Süd.

Downloaded from https://pubs.geoscienceworld.org/eurjmin/article-pdf/30/3/621/4346636/ejm_30_3_0621_0634_grey_2707_online.pdf
by University of Arizona user
on 27 September 2018

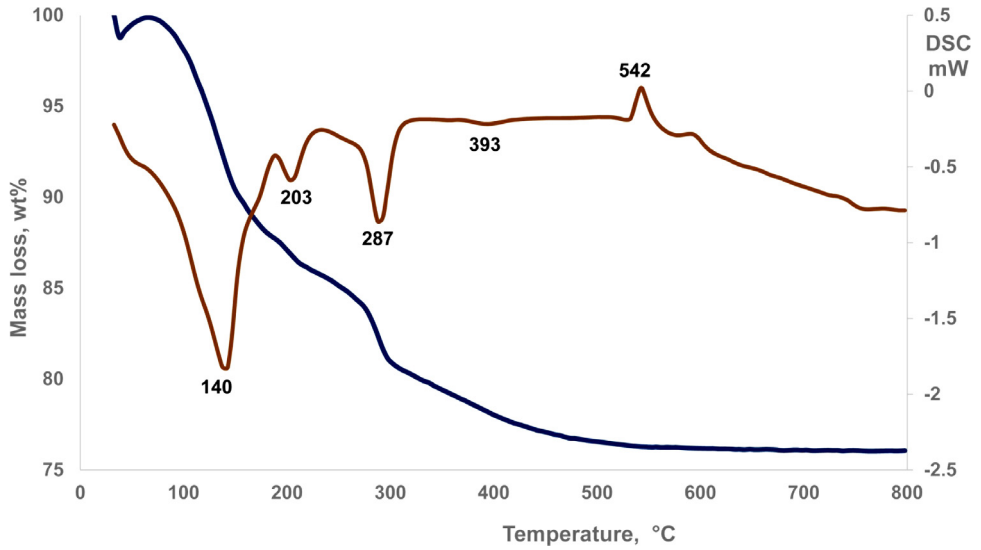

Fig. 5. Thermogravimetric and differential scanning calorimetry curves for green SGM from Hagendorf Süd, sample IGC-11.

2.4. Thermal analyses

Thermogravimetric analyses were performed on ~20 mg samples of pure SGMs from samples IGC-11 and IGC-14 using a Netzsch STA 449 F1 Jupiter Simultaneous TGA/DSC thermal analyser. The analyses were run in argon, with a ramp rate of 10 °C/min, between 30 and 800 °C. Evolved gas analyses were made using a coupled Thermostar Pfeiffer mass spectrometer (MS). Plots of the TGA and DSC curves for the SGM in IGC-11 are given in Fig. 5.

2.5. X-ray data collections and refinements

The PXRD patterns for Hagendorf Süd SGMs were collected in the 2θ range 6–80° using a Philips diffractometer with graphite monochromator, and employing Co*K*α radiation. The cell parameters were refined using the Rietveld program FULLPROF (Rodriguez-Carvajal, 1990). Room-temperature unit-cell parameters for the two Palermo samples were obtained by refinement of single-crystal data collected on a Rigaku R-Axis Rapid II curved-imaging-plate microdiffractometer utilising monochromatised Mo*K*α radiation. The same two crystals were subsequently used for synchrotron single-crystal data collections.

Synchrotron single-crystal data collections were conducted on the macromolecular beam line MX2 of the Australian Synchrotron. Data were collected at 100 K using an ADSC Quantum 315r detector and monochromatic radiation with a wavelength of 0.7107 Å. A phi scan was employed with framewidths of 1° and a counting time per frame of 1 s. The intensity data sets were processed to produce data files, which were analysed in WinGX (Farrugia, 1999). The refinements were made using JANA2006 (Petříček *et al.*, 2014).

The synchrotron data sets were refined using the published coordinates for schoonerite (Kampf, 1977) in space group *Pbam* as a starting model. Elevated displacement parameters for the $^{[5]}$Zn site in the oxidized samples, IGC-14 and Palermo red, and subsequent difference Fourier maps, showed a partitioning of the Zn from the $^{[5]}$Zn site to an adjacent tetrahedral site $^{[4]}$Zn, as found for wilhelmgümbelite and schmidite (Grey *et al.*, 2017a and b). The two sites are separated by 1.0 Å. Free refinement of the site occupancies for the two sites gave combined Zn occupancies less than one. Bond-valence sums (BVS) at the two sites were >2, more so for the $^{[4]}$Zn site. Minor Fe^{3+} was added to both sites, consistent with the BVS, and this resulted in refined site occupancies close to 1 for $^{[5]}$Zn/Fe + $^{[4]}$Zn/Fe.

The establishment of site occupancies for the metal atom sites *M*1, *M*2, *M*3 and *M*4 poses difficulties because of the presence of three major constituents, Zn, Mn and Fe, the possibility of different valence states for Fe and Mn, as well as the presence of cation vacancies as reported for wilhelmgümbelite and schmidite (Grey *et al.*, 2017a and b). In practice, a number of favourable circumstances helped to overcome the difficulties, at least for the highly oxidized samples for which Mössbauer spectroscopy shows that Fe is predominantly Fe^{3+}. Firstly, refinements of all data sets, including those for wilhelmgümbelite and schmidite, show that site *M*4 contains only Fe^{3+} (no Mn or Zn) and the $^{[4]}$Zn/$^{[5]}$Zn sites contain predominantly Zn. Secondly, previous structure analyses of wilhelmgümbelite and schmidite (Grey *et al.*, 2017a and b) have shown that the cation deficiency occurs at one site, *M*3, and is correlated with the extent of partitioning of Zn from the $^{[5]}$Zn site into the $^{[4]}$Zn site (cation vacancy concentration at *M*3 equals the concentration of $^{[4]}$Zn), so the vacancy concentration at *M*3 is well determined. Thirdly, there is sufficient atomic number contrast between Zn and Fe/Mn to allow the zinc content of the *M*1 to *M*3 sites to be determined by site-occupancy refinement. Minor Mg was located at the *M*1 site because preliminary refinements showed that the samples with the highest Mg contents consistently gave a lower site scattering at *M*1 than provided by Fe/Mn.

Downloaded from https://pubs.geoscienceworld.org/eurjmin/article-pdf/30/3/621/4346636/ejm_30_3_0621_0634_grey_2707_online.pdf
by University of Arizona user
on 27 September 2018

Table 4. Data collection and refinement details.

	IGC-14	Palermo red	Palermo brown	IGC-2	IGC-11
Unit-cell dimensions, Å	$a = 11.044(1)$	11.047(2)	11.136(2)	11.155(1)	11.176(1)
(100 K)	$b = 25.431(1)$	25.414(5)	25.575(5)	25.517(2)	25.477(1)
	$c = 6.412(1)$	6.422(1)	6.435(1)	6.432(1)	6.441(1)
Volume, Å^3	1800.9(2)	1803.0(6)	1832.7(7)	1830.8(3)	1834.0(3)
Density (calc.), g/cm^3	2.81	2.76	2.74	2.75	2.75
Crystal size, mm^3	$0.080 \times 0.030 \times 0.010$	$0.250 \times 0.070 \times 0.005$	$0.080 \times 0.080 \times 0.005$	$0.090 \times 0.040 \times 0.005$	$0.100 \times 0.030 \times 0.007$
Absorption coefficient, mm^{-1}	4.66	4.48	4.49	4.59	4.47
SADABS, T_{min}/T_{max}	0.35, 0.44	0.65, 0.75	0.51, 0.75	0.22, 0.43	0.35, 0.44
Reflections collected, R_{int}	36 364, 0.028	31 072, 0.020	26 404, 0.085	34 400, 0.103	36 496, 0.045
Data resolution for refine, Å	0.7	0.7	0.95	0.7	0.7
Unique refl.: all, $I>2\sigma(I)$]	2142, 2059	2461. 2402	1121, 1064	2239, 2150	2669. 2594
Parameters, restraints, constraints	197, 16, 58	165, 0, 44	162, 0, 39	163, 0, 50	193, 16, 53
Final R indices [$I>2\sigma(I)$]	$R_{obs} = 0.028$, $wR_{obs} = 0.029$	$R_{obs} = 0.038$, $wR_{obs} = 0.039$	$R_{obs} = 0.046$, $wR_{obs} = 0.047$	$R_{obs} = 0.050$, $wR_{obs} = 0.051$	$R_{obs} = 0.038$ $wR_{obs} = 0.039$
R indices (all data)	$R_{obs} = 0.028$, $wR_{obs} = 0.028$	$R_{obs} = 0.051$, $wR_{obs} = 0.051$	$R_{obs} = 0.057$, $wR_{obs} = 0.057$	$R_{obs} = 0.062$, $wR_{obs} = 0.062$	$R_{obs} = 0.046$, $wR_{obs} = 0.046$
GofF	4.57	4.15	3.62	3.41	3.36
Largest diff. peak, hole (eÅ^{-3})	0.57, −0.73	1.63, −1.53	1.24, −0.76	1.85, −1.08	1.55, −2.23

Table 5. Refined coordinates, equivalent isotropic displacement parameters (Å^2) and BVS values for IGC-11 and IGC-14.

	Green SGM, IGC-11					Red SGM, IGC-14				
Atom	x	y	z	U_{eq}	BVS	x	y	z	U_{eq}	*BVS*
$^{[5]}$Zn	0.25	0.103737(13)	0.85020(5)	0.00834(12)	2.01	0.25	0.103282(14)	0.84992(6)	0.01812(12)	2.13
$^{[4]}$Zn	absent					0.25	0.06344(10)	0.8835(3)	0.0267(8)	2.28
*M*1	0.25	0.416379(14)	0.22797(6)	0.00746(14)	2.04	0.25	0.415969(13)	0.22762(5)	0.01667(12)	2.41
*M*2	0	0.25	0.07564(6)	0.00653(14)	2.02	0	0.25	0.08912(5)	0.01392(11)	2.45
*M*3	0	0.25	0.58612(6)	0.00684(14)	2.06	0	0.25	0.57272(6)	0.01436(12)	2.15
*M*4	0.25	0.185177(14)	0.32788(5)	0.00534(12)	3.03	0.25	0.188174(11)	0.32529(4)	0.01070(9)	3.15
P1	0.02897(5)	0.118979(17)	0.14218(7)	0.00625(14)	4.92	0.03090(4)	0.119027(15)	0.14193(6)	0.01151(11)	4.94
P2	0.25	0.21625(2)	0.82358(10)	0.00547(18)	4.89	0.25	0.21681(2)	0.82660(8)	0.01023(15)	4.91
O1	0.02736(15)	0.32980(5)	0.0608(2)	0.0106(4)	1.69	0.02395(12)	0.32950(4)	0.05614(18)	0.0173(3)	1.67
O2	0.06588(15)	0.41780(5)	0.2314(2)	0.0093(4)	1.73	0.06765(12)	0.41675(5)	0.23048(19)	0.0178(3)	1.80
O3	0.09123(14)	0.09098(5)	0.9596(2)	0.0112(4)	1.78	0.09233(12)	0.08950(5)	0.96144(19)	0.0192(4)	1.82
O4	0.11946(14)	0.13180(5)	0.3177(2)	0.0081(4)	1.72	0.12163(11)	0.13121(5)	0.31931(16)	0.0149(3)	1.69
O5	0.25	0.18132(7)	0.0194(3)	0.0087(5)	1.99	0.25	0.18012(6)	0.0173(2)	0.0149(4)	1.99
O6	0.25	0.17586(7)	0.6423(3)	0.0073(5)	1.87	0.25	0.17923(7)	0.6372(2)	0.0180(5)	1.86
O7	0.13582(14)	0.24959(5)	0.8186(2)	0.0082(4)	1.91	0.13321(13)	0.24990(5)	0.8283(2)	0.0211(4)	1.77
Oh	0.12568(14)	0.24306(5)	0.3370(2)	0.0080(4)	1.17	0.12248(13)	0.24229(5)	0.32645(19)	0.0224(4)	1.38
Ow1	0.02782(14)	0.33468(5)	0.6182(2)	0.0089(4)	0.32	0.02710(13)	0.33226(6)	0.6161(2)	0.0220(4)	0.31
Ow2	0.25	0.34418(7)	0.4357(3)	0.0101(5)	0.26	0.25	0.34551(7)	0.4233(3)	0.0216(5)	0.33
Ow3	0.25	0.36479(8)	0.9541(3)	0.0103(5)	0.31	0.25	0.36505(7)	0.9586(3)	0.0210(5)	0.36
Ow4	0.25	0.46162(8)	0.5169(3)	0.0108(5)	0.32	0.25	0.46111(7)	0.5090(3)	0.0215(5)	0.38
Ow5	0.25	0.48980(8)	0.0465(3)	0.0124(6)	0.32	0.25	0.48719(8)	0.0473(3)	0.0244(6)	0.45
Ow6	0.25	0.06320(10)	0.5898(4)	0.0469(13)	0.51	0.25	0.06433(9)	0.5887(4)	0.0442(9)	0.55
Ow7	0.05741(15)	0.48228(5)	0.7680(2)	0.0123(4)		0.05842(13)	0.48205(5)	0.7633(2)	0.0238(4)	
Hoh	0.155(3)	0.2731(9)	0.344(5)	0.020(3)		absent				
H1a	−0.021(2)	0.3537(11)	0.551(4)	0.020(3)		−0.028(2)	0.3507(11)	0.558(4)	0.041(3)	
H1b	0.021(3)	0.3411(11)	0.749(3)	0.020(3)		0.027(2)	0.3377(12)	0.747(3)	0.041(3)	
H2	0.3113(13)	0.3471(12)	0.5100(17)	0.020(3)		0.3130(12)	0.3470(12)	0.4997(16)	0.041(3)	
H3	0.3129(12)	0.3454(4)	0.963(5)	0.020(3)		0.3126(12)	0.3463(5)	0.976(5)	0.041(3)	
H4	0.3122(13)	0.4635(13)	0.5929(17)	0.020(3)		0.3132(12)	0.4677(12)	0.581(2)	0.041(3)	
H5	0.3131(13)	0.4902(12)	−0.0309(16)	0.020(3)		0.3130(13)	0.4923(11)	−0.027(2)	0.041(3)	
H6	0.305(5)	0.072(3)	0.671(10)	0.020(3)		0.3124(13)	0.0478(7)	0.627(4)	0.041(3)	
H7a	0.012(2)	0.4583(9)	0.817(5)	0.020(3)		0.0021(18)	0.4588(8)	0.761(5)	0.041(3)	
H7b	0.017(2)	0.5096(8)	0.748(6)	0.020(3)		0.027(2)	0.5127(7)	0.750(5)	0.041(3)	

Downloaded from https://pubs.geoscienceworld.org/eurjmin/article-pdf/30/3/621/4346636/ejm_30_3_0621_0634_grey_2707_online.pdf
by University of Arizona user
on 27 September 2018

Table 6. Metal atom site occupancies from the current five refinements, together with results from previous refinements for Wilhelmgümbelite and Schmidite.

	Wilhelmgümbelite	Schmidite	IGC-14	Palermo red	Palermo brown	IGC-2	IGC-11
$^{[5]}$Zn	0.70 Zn	0.80 Zn	0.68 Zn + 0.16 Fe^{3+}	0.72 Zn + 0.08 Fe^{3+}	0.89 Zn + 0.06 Fe^{3+}	0.86 Zn + 0.14 Fe^{3+}	0.86 Zn + 0.1 Fe^{2+}
$^{[4]}$Zn	0.30 Zn	0.20 Zn	0.10 Zn + 0.06 Fe^{3+}	0.16 Zn + 0.04 Fe^{3+}			
*M*1	0.73 Fe^{3+} +	0.12 Zn +	0.06 Mg + 0.06 Zn +	0.12 Mg +	0.13 Mg + 0.11 Fe^{3+} +	0.06 Mg + 0.02 Zn +	0.06 Mg + 0.04 Fe^{3+} +
	0.27 Mn^{2+}	0.57 Fe^{3+} +	0.47 Fe^{3+} + 0.41 Mn^{2+}	0.57 Fe^{3+} + 0.31 Mn^{2+}	0.44 Fe^{2+} + 0.32 Mn^{2+}	0.08 Fe^{3+} + 0.44 Fe^{2+} + 0.40 Mn^{2+}	0.50 Fe^{2+} + 0.40 Mn^{2+}
		0.31 Mn^{2+}					
*M*2	0.25 Zn +	0.65 Fe^{3+} +	0.1 Zn + 0.51 Fe^{3+} +	0.02 Zn +	0.03 Zn + 0.19 Fe^{3+} +	0.05 Zn + 0.03 Fe^{3+} +	0.08 Zn + 0.02 Fe^{3+} +
	0.60 Fe^{3+} +	0.35 Mn^{2}	0.39 Mn^{2+}	0.62 Fe^{3+} + 0.36 Mn^{2+}	0.46 Fe^{2+} + 0.32 Mn^{2+}	0.52 Fe^{2+} + 0.40 Mn^{2+}	0.50 Fe^{2+} + 0.40 Mn^{2+}
	0.15 Fe^{2+}						
*M*3	0.25 Zn +	0.45 Zn +	0.24 Zn + 0.13 Fe^{3+} +	0.25 Zn +	0.30 Zn + 0.06 Fe^{3+} +	0.30 Zn + 0.08 Fe^{3+} +	0.08 Zn + 0.06 Fe^{3+} +
	0.45 Fe^{2+} +	0.11 Fe^{3+} + 0.24 Mn^{2+}	0.08 Fe^{2+} +	0.05 Fe^{3+} + 0.27 Fe^{2+}	0.20 Fe^{2+} +	0.22 Fe^{2+} + 0.40 Mn^{2+}	0.46 Fe^{2+} + 0.40 Mn^{2+}
	0.30 Vac.	+ 0.20 Vac.	0.40 Mn^{2+} + 0.15 Vac.	+ 0.23 Mn^{2+}	0.32 Mn^{2+} + 0.12 Vac.		
				+ 0.20 Vac.			
*M*4	Fe^{3+}	0.94 Fe^{3+} + 0.06 Al	Fe^{3+}	Fe^{3+}	Fe^{3+}	Fe^{3+}	Fe^{3+}

The remaining major consideration is the valence state of Mn in the sites *M*1 to *M*3. Redox potentials for Mn^{2+}/Mn^{3+} and Fe^{2+}/Fe^{3+} dictate that Mn^{3+} cannot exist stably in the presence of Fe^{2+}. All SGM minerals studied contain some Fe^{2+}, so it might be expected that only Mn^{2+} will be present, although a doubt remains for the highly oxidised minerals. A more direct argument in support of Mn^{2+} comes from the experimental bond distances for the *M*1–*M*3 sites. The total number of Fe^{2+}, Fe^{3+}, Zn, Mg and Mn^{n+} cations in the combined *M*1 + *M*2 + *M*3 sites are known from the EMP analyses and Mössbauer results. They can be used to weight the individual mean octahedral <*M*–O> distances (calculated from BV parameters for Fe^{2+}, Fe^{3+}, etc) and equate this weighted distance to the experimentally determined <*M*–O> distance from the structure refinement, averaged over the *M*1–*M*3 sites. The only unknown is the value of *n* for the Mn oxidation state. Applying this approach to schmidite, which is the most oxidized of the SGMs, gives a value for $<Mn^{n+}–O>$ of 2.22. This compares with values of 2.20 for $<Mn^{2+}–O>$ and 2.015 for $<Mn^{3+}–O>$, calculated for undistorted octahedra using the BVS parameters of Brown & Altermatt (1985). This is strong evidence for the Mn being predominantly, if not exclusively, in the divalent state. The calculation details are given in Appendix A.

The refinement approach for the oxidized samples started with 50/50 Fe/Mn plus Zn in the sites *M*1, *M*2 and *M*3, and the Zn site occupancy of the three sites was refined to establish the Zn contents. There is a large difference in the ionic radii of Mn^{2+} and Fe^{3+}, so that once the Zn occupancy had been determined, the amounts of Mn^{2+} and Fe^{3+} in sites *M*1, *M*2 and *M*3 could be determined from the calculated BVS for the sites. A correction was made to the determined Fe^{3+}/Mn^{2+} ratio for systematic BVS errors when mixed-valent cations occupy the same site, following the procedure described by Bosi (2004). The validity of the approach was independently checked by confirming that the obtained Mn, Fe and Zn values, summed over the sites *M*1–*M*3, matched with the results from the EMP analyses.

For the samples containing high levels of Fe^{2+}, the assignment of site occupancies was not so straightforward. The similarity in both scattering strength and bond distances for Fe^{2+} and Mn^{2+} prevented unambiguous assignment of these two cations. We used the assumption that the uniform distribution of Mn^{2+} in sites *M*1, *M*2 and *M*3 that was found for oxidized samples applied also to the more reduced samples. With the Mn^{2+} thus assigned, and the Zn contents determined by site occupancy refinement, calculated BVS values from the refined bond distances were then used to determine the Fe^{2+}/Fe^{3+} contents for the sites *M*1, *M*2 and *M*3. The resulting overall Fe^{3+}/(Fe^{2+} + Fe^{3+}) ratio could then be checked for consistency against the analysed value. The latter was obtained from Mössbauer spectroscopy for the Hagendorf Süd samples. The quantities of the SGMs present on the Palermo sample were too small to obtain Mössbauer spectra or chemical

Downloaded from https://pubs.geoscienceworld.org/eurjmin/article-pdf/30/3/621/4346636/ejm_30_3_0621_0634_grey_2707_online.pdf
by University of Arizona user
on 27 September 2018

Table 7. Room-temperature cell parameters, ferric iron fractions and bond distances (Å) for SGMs.

	Schmidite IGC-1	IGC-14	Palermo red	Wilhelmgümbelite IGC-34	Palermo brown	IGC-2	IGC-11	Schoonerite (Kampf, 1977)
a	11.059(1)	11.082(1)	11.085(1)	11.010(2)	11.148(2)	11.165(1)	11.194(1)	11.119(4)
b	25.452(1)	25.498(2)	25.500(1)	25.333(3)	25.609(4)	25.602(1)	25.552(1)	25.546(11)
c	6.427(1)	6.436(1)	6.436(1)	6.421(1)	6.455(1)	6.442(1)	6.460(1)	6.437(3)
$Fe^{3+}/(Fe^{2+}+Fe^{3+})$	0.98	0.97	0.90	0.76	0.66	0.68	0.46	0.33
$^{[5]}$Zn–O3 (×2)	1.919	1.915	1.921	1.934	1.926	1.921	1.936	1.91(1)
–Ow6	1.953	1.946	1.947	1.937	1.955	1.957	1.970	1.99(2)
–O5	2.217	2.230	2.226	2.191	2.278	2.263	2.257	2.28(2)
–O6	2.377	2.364	2.366	2.469	2.305	2.277	2.274	2.38(2)
Av.	2.077	2.074	2.076	2.093	2.078	2.068	2.075	2.094
$^{[4]}$Zn–O3 (×2)	1.905	1.929	1.922	1.917	Absent	Absent	Absent	Absent
–Ow5	2.096	1.989	2.031	2.106				
–Ow6	1.909	1.890	1.926	1.886				
Av.	1.954	1.934	1.950	1.957				
*M*1–O2 (×2)*	1.998	2.014	1.989	1.991	2.037	2.051	2.058	2.03(1)
–Ow2	2.186	2.187	2.168	2.133	2.236	2.265	2.275	2.24(2)
–Ow3	2.142	2.157	2.148	2.096	2.195	2.199	2.200	2.22(2)
–Ow4	2.148	2.138	2.111	2.073	2.190	2.191	2.189	2.22(2)
–Ow5	2.139	2.149	2.124	2.074	2.187	2.186	2.206	2.23(2)
Av.	2.102	2.110	2.088	2.060	2.147	2.157	2.164	2.162
*M*2–O1 (×2)	2.040	2.050	2.032	2.058	2.057	2.067	2.058	2.02(1)
–O7 (×2)	2.221	2.227	2.219	2.124	2.260	2.243	2.246	2.27(1)
–Oh (×2)	2.023	2.045	2.024	2.011	2.103	2.184	2.199	2.08(1)
Av.	2.095	2.107	2.092	2.064	2.140	2.165	2.168	2.123
*M*3–O7 (×2)	2.206	2.202	2.215	2.235	2.163	2.129	2.132	2.20(1)
–Oh (×2)	2.101	2.088	2.088	2.132	2.101	2.124	2.139	2.11(1)
–Ow1 (×2)	2.140	2.132	2.121	2.085	2.168	2.178	2.190	2.15(1)
Av.	2.149	2.141	2.141	2.151	2.144	2.144	2.154	2.153
*M*4–Oh (×2)	1.983	1.969	1.978	1.984	2.009	2.032	2.027	2.00(1)
–O4 (×2)	2.034	2.027	2.042	2.010	2.028	1.985	1.996	2.00(1)
–O5	1.993	1.985	1.996	1.994	1.991	1.979	1.989	2.00(1)
–O6	2.004	2.013	2.022	1.984	2.037	2.032	2.039	2.00(1)
Av.	2.005	1.998	2.010	1.996	2.017	2.008	2.012	2.000

* *M*–O e.s.d.s are in the range 0.001–0.005 except for wilhelmgümbelite (0.007–0.012).

analysis for $Fe^{3+}/(Fe^{2+}+Fe^{3+})$, but we were able to obtain reasonable estimates from a linear relationship that was established between the *a* cell parameter and the mean bond length for the $M1+M2+M3$ sites, as described in Appendix B.

Refinements with anisotropic displacement parameters converged satisfactorily, and H atoms could be located unambiguously from difference-Fourier maps in the case of SGM crystals from samples IGC-11 and IGC-14. The H atoms were refined with soft restraints, O–H = 0.85(2) Å and H–O–H = 109.5(2)°. The distance used in the restraint represents an average of unrefined O–H distances obtained from the difference-Fourier maps. A single isotropic displacement parameter was refined for the H atoms. Single-crystal data collection and refinement details are given in Table 4. The refined coordinates and equivalent isotropic displacement parameters for SGM crystals from samples IGC-11 and IGC-14 are given in Table 5. The results for crystals from IGC-2, Palermo red and Palermo brown samples are freely available as Supplementary Material linked to the article on the GSW website of the journal, https://pubs.geoscienceworld.org/eurjmin/, as are anisotropic displacement parameters for IGC-11 and IGC-14. The site-occupancies for all metal atom sites are given in Table 6 for the five current refinements as well as for previous refinements of wilhelmgümbelite and schmidite. Polyhedral bond lengths are given in Table 7 and H bonds for SGMs from samples IGC-11 and IGC-14 in Table 8.

Downloaded from https://pubs.geoscienceworld.org/eurjmin/article-pdf/30/3/621/4346636/ejm_30_3_0621_0634_grey_2707_online.pdf
by University of Arizona user
on 27 September 2018

Table 8. Hydrogen bonds for red (IGC-14) and green (IGC-11) SGMs.

D–H···A	d(D–H)	d(H···A)	d(D···A)	<(DHA)
IGC–14				
Ow1–H1a···O4	0.86(3)	1.90(2)	2.680(2)	150(2)
Ow1–H1b···O1	0.85(2)	1.99(2)	2.823(2)	165(3)
Ow2–H2···Ow1	0.85(1)	1.95(1)	2.775(2)	162(2)
Ow3–H3···O1	0.85(1)	1.92(1)	2.728(2)	158(1)
Ow4–H4···Ow7	0.85(1)	1.87(1)	2.724(2)	174(1)
Ow5–H5···Ow7	0.85(1)	1.97(1)	2.795(2)	161(2)
Ow6–H6···Ow4	0.84(2)	2.47(2)	2.699(3)	97(1)
Ow7–H7a···O3	0.86(2)	2.06(3)	2.774(2)	140(3)
Ow7vH7b···O2	0.86(2)	2.08(2)	2.926(2)	169(3)
IGC-11				
Oh–Hoh···Ow2	0.83(2)	2.18(3)	2.995(2)	165(3)
Ow1–H1a···O4	0.85(3)	1.90(2)	2.681(2)	153(2)
Ow1–H1b···O1	0.86(2)	2.03(2)	2.853(2)	159(3)
Ow2–H2···Ow1	0.84(1)	1.95(1)	2.809(2)	171(2)
Ow3–H3···O1	0.86(1)	1.93(2)	2.731(2)	153(2)
Ow4–H4···Ow7	0.85(1)	1.90(1)	2.743(2)	168(3)
Ow5–H5···Ow7	0.86(1)	1.95(1)	2.809(2)	171(2)
Ow6–H6···O3	0.84(6)	2.24(6)	3.053(3)	162(5)
Ow7–H7a···O3	0.85(3)	1.94(3)	2.787(2)	173(3)
Ow7–H7b···O2	0.84(2)	2.07(2)	2.895(2)	166(3)

3. Results and discussion

3.1. EMP results and SGM compositions

The EMP analyses are reported in Table 1. Empirical formulae have been calculated from the EMP analyses combined with the FeO/Fe_2O_3 ratios and are given in Table 1, normalised to 3P and 23 anions (ideally 12 $O^{2-} + 2\ OH^- + 9\ H_2O$). Charge balance was achieved by adjustment of the hydroxyl content. The structure refinement results suggest that some replacement of O^{2-} for OH^- occurs in the more oxidized samples, but this is small and variable and so is not shown in the formulae in Table 1. Also shown in Table 1 are the sums of the metal atoms in the empirical formulae, which are all lower than the ideal value of 5.

The EMP analyses reported in Table 1 show only minor variations in the major elements, Zn, Mn and Fe. Similar contents of these elements are found not just for samples taken at different levels in the mine at Hagendorf Süd, but also for the samples from the Palermo No.1 pegmatite. Similar small elemental variations occur for the minerals rockbridgeite and jahnsite that are intimately associated with the Hagendorf Süd schoonerite minerals, as seen from the results in Table 2. The jahnsite analyses correspond to jahnsite-(CaMnFe), while the rockbridgeite is both Zn- and Mn-bearing. Moore (1982) has noted the similarity in the phosphate assemblages at Palermo No.1 and Hagendorf Süd. At both localities, triphylite, $Li(Fe^{2+}, Mn^{2+})PO_4$, is considered to be the primary phosphate precursor for the formation of schoonerite and most other secondary phosphates. The Mn/(Mn + Fe) atomic ratio of the triphylite is almost the same at both localities, averaging ~0.25 (Keller *et al.*, 1994; Moore, 2000), indicating similar degrees of fractionation of the pegmatite. Different authors have noted that secondary phosphate phase assemblages formed by metasomatic and hydrothermal alteration of triphylite often preserve the original Mn/(Mn + Fe) atomic ratio (Moore, 1982; Fransolet, 2007). The EMP results bear this out. The two Palermo schoonerites have ratios of 0.27 and 0.28, close to the value for Palermo No.1 triphylite. The Hagendorf Süd samples have ratios in the range from 0.26 to 0.31 a little higher than the parent triphylite. In this case, however, the whole assemblage of schoonerite + rockbridgeite + jahnsite has to be considered. The Mn/(Mn + Fe) atomic ratios in the analysed rockbridgeites and jahnsites are in the ranges from 0.08 to 0.11 and from 0.35 to 38, lower and higher, respectively, than for schoonerite.

In his paper on the paragenesis of the phosphate minerals of the Hagendorf pegmatite, Mücke (1981) located schoonerite in his Table 2 (rockbridgeite subparageneses), under paragenesis IID1. He considered that both oxidized and reduced forms of schoonerite were derived from the reaction of rockbridgeite (itself a transformation product of triphylite) with solution-mobilized Zn from sphalerite. The Hagendorf Süd samples used in the current study (IGC-2, IGC-11 and IGC-14), belong to Mücke's paragenesis IID1. In contrast, schmidite and wilhelmgümbelite both belong to Mücke's classification IC (rockbridgeite-free subparagenesis), comprising minerals that he considered were derived from the reaction of phosphophyllite with hydrothermal fluid elements including Zn.

3.2. Mössbauer spectroscopy and thermal analyses

Mössbauer spectra were obtained primarily to determine the overall oxidation state of the iron ($Fe^{3+}/(Fe^{2+} + Fe^{3+})$ ratio) in the Hagendorf Süd samples, but some comments can be made about site assignments for Fe^{3+}. A feature common to all minerals with the schoonerite structure is the ordering of Fe^{3+} into site *M*4. This is the least distorted of the metal atom sites. For each of the samples in Table 3, the Fe^{3+} doublet with the smallest quadrupole splitting, $\Delta = 0.5$ mm/s, has an area corresponding to ~1 Fe^{3+} per formula unit, and can be unambiguously assigned to *M*4. For the almost fully oxidized SGM in sample IGC-14, sites *M*1 and *M*2 each contain ~0.5 Fe^{3+}, whereas site *M*3 contains only 0.13 Fe^{3+} (Table 6). These facts allow the intermediate doublet with $\Delta = 0.9$ mm/s to be assigned to Fe^{3+} in *M*1 + *M*2 and the doublet with $\Delta = 1.3$ mm/s to be assigned to Fe^{3+} in *M*3. In the spectrum for the SGM in sample IGC-2, a broad doublet with intermediate $\Delta = 1.1$ mm/s must contain unresolved contributions from *M*1, *M*2 and *M*3, while in the spectrum for the most reduced SGM, in the sample IGC-11, the Fe^{3+} contributions from sites *M*1, *M*2 and *M*3 are not sufficiently high to be resolved from the main *M*4 doublet.

Downloaded from https://pubs.geoscienceworld.org/eurjmin/article-pdf/30/3/621/4346636/ejm_30_3_0621_0634_grey_2707_online.pdf
by University of Arizona user
on 27 September 2018

We did not attempt assignment of the Fe^{2+} doublets. This is because complications arise due to possibly severe next-nearest-neighbour (NNN) effects (Li & Shinno, 1997) resulting from the mixed site occupancies. Multiple Fe^{2+} doublets with low areas were fitted for the SGM in IGC-2, while for IGC-11, the doublet with $\Delta = 2.11$ mm/s has a very large Gaussian width that may correspond to a number of weak doublets with varying Δ values.

The different types of water in the structure were determined directly from thermal analysis, with mass spectrometry confirming that the endotherms corresponded to water evolution. The TG and DSC curves in Fig. 5 for the most reduced SGM, in sample IGC-11, can be interpreted with the aid of the empirical formula, Table 1, and the structure refinement results. Sharp water-loss endotherms at temperatures of 140, 203 and 287 °C are associated with mass losses of 12.2% (30–186 °C), 2.5% (186–231 °C) and 5.5% (231–300 °C), respectively. A weak broad endotherm centred at 393 °C is associated with a mass loss of 3.6%. A sharp exotherm at 542 °C is interpreted to indicate recrystallization of the dehydrated phase. The mass loss associated with the first endotherm corresponds to the loss of 5 H_2O. These would include the interlayer water, $2 \times$ Ow7, and the water molecules Ow2, Ow3 and Ow5 coordinated to *M*1 with long bonds in the range from 2.20 to 2.275 Å, see Table 7. Loss of the fourth water molecule coordinated to *M*1, Ow4 (*M*1–Ow4 = 2.186 Å), is linked to the endotherm at 203 °C. The mass loss associated with the third endotherm corresponds to just over 2 water molecules, and can be associated with $2 \times$ Ow1 which are coordinated to *M*2. Loss of the most tightly bound water molecule, Ow6 ($^{[5]}$Zn–Ow6 = 1.97 Å) together with loss of hydroxyl groups as water occurs gradually from 230 up to ~600 °C.

The DSC curve for the oxidized SGM in sample IGC-14 was not as well resolved as that for IGC-11, most likely due to the mixing of variable amounts of OH^- groups and H_2O at anion sites. In place of the three endotherms observed for IGC-11, only a single strong endotherm was observed for IGC-14, centred at 140 °C, with shoulders at ~90 and 170 °C. Above 270 °C, only very weak broad features are observed in the DSC curve. The mass loss from 30 to 270 °C of 16.8% corresponds to the loss of ~6 H_2O, *i.e.* interlayer Ow7 × 2 plus the four water molecules coordinated to *M*1. Above 270 °C, the mass losses due to the remaining coordinated water molecules and hydroxyl groups are gradual and undifferentiated. This can be explained by the mixing of Fe^{3+} with Mn^{2+} and Zn at the metal sites together with vacancies in *M*3 in IGC-14, resulting in considerable disorder in the location of coordinated water and hydroxyl groups. Such disorder is evident in the elevated isotropic displacement parameter for H atoms in IGC-14 of 0.041(3) $Å^2$, compared to a value of 0.020(3) $Å^2$ for the H atoms in IGC-11.

3.3. H-bonding

A comparison of the hydrogen bonding in reduced (IGC-11) and oxidized (IGC-14) SGMs is given in Table 8. For the reduced IGC-11 sample, the H atoms were all well-determined and the H-bonding corresponds to that reported by Kampf (1977) for schoonerite. Kampf did not locate H atoms, but based the H-bonding on geometrical grounds. The results agree for all bonds except those associated with Ow6. Kampf (1977) proposed a bifurcated bond between Ow6 and O4 as well as a bond from Ow6 to Ow4, whereas we found only a weak H-bond from Ow6 to O3 in IGC-11. Ow6 is unusual in being the only atom in the schoonerite structure having highly anisotropic displacement parameters, with $U^{11} = 0.123(4)$ in IGC-11 and 0.086(2) in IGC-14. These correspond to mean-square displacements along [100] of 0.35 and 0.29 Å respectively, and indicate that Ow6 is disordered over sites on either side of the mirror plane at $x = ¼$. Splitting the Ow6 into two sites gave an increase in the *R* factor, suggesting that the disorder is dynamic.

The main difference between the reduced and oxidized SGMs regarding the H bonds, is that an H atom associated with the OH site could not be located in the difference Fourier map for the oxidized mineral. The failure to locate H at the OH site was also encountered in our refinement of schmidite (Grey *et al.*, 2017b). Pairs of OH atoms form a shared edge between the *M*2- and *M*3-centred octahedra and coordinate also to *M*4. As seen from Table 7, the *M*2–OH bonds undergo a marked shortening on oxidation, from 2.206 Å in IGC-11 to 2.045 Å in IGC-14. This is by far the largest bond-length adjustment accompanying oxidation, and suggests that OH^- is converted, at least partially, to O^{2-} during the oxidation. BVS values at the OH site were calculated to be typically 1.3–1.4 for the oxidized samples, compared with 1.1–1.2 for the more reduced samples, so the site would appear to be still predominantly OH^-.

3.4. Crystallochemical considerations

Tables 6 and 7 summarise the main crystallochemical changes found in the current structure refinements, as well as for refinements previously conducted on schoonerite, wilhelmgümbelite and schmidite (Kampf, 1977; Grey *et al.*, 2017a and b). The results in Table 7 are ordered in terms of the extent of oxidation of the minerals, given by the fraction of Fe as Fe^{3+}, $Fe^{3+}/(Fe^{2+} + Fe^{3+})$. This compositional factor is associated with a significant structural change whereby, for increasing Fe^{3+} content, the ordering of Zn in the $^{[5]}$Zn site changes to a partitioning of the Zn between the $^{[5]}$Zn site and an adjacent tetrahedral site, $^{[4]}$Zn. The tetrahedral site is outlined by the dashed lines in Fig. 1. It shares a face, O3-O3-Ow6, with the $^{[5]}$Zn site and the relocation of the Zn involves a displacement through the face by ~1 Å. As seen from Table 7, SGMs with <70% of the iron as Fe^{3+} have Zn in the $^{[5]}$Zn site only, whereas all more oxidized samples have the Zn distributed between the two sites. The site occupancy results in Table 6 show that oxidized minerals displaying Zn partitioning have all iron as Fe^{3+} in the *M*1 and *M*2 sites, whereas the minerals without partitioning have the iron predominantly as Fe^{2+} (>80%) in these two sites. The extent of partitioning of the Zn from $^{[5]}$Zn to $^{[4]}$Zn is

Downloaded from https://pubs.geoscienceworld.org/eurjmin/article-pdf/30/3/621/4346636/ejm_30_3_0621_0634_grey_2707_online.pdf
by University of Arizona user
on 27 September 2018

relatively limited, in the 16–30% range. The low-Mn mineral, wilhelmgümbelite, has the greatest partitioning and also has the highest levels of Fe^{3+} in the *M*1 and *M*2 sites.

In the structure refinement of wilhelmgümbelite (Grey *et al.*, 2017a), an apparent correlation was noted between the extent of partitioning of the Zn (30%) and the cation deficiency in the *M*3 site (30%). This correlation has been found to hold for schmidite and for the two oxidized minerals in the current study, IGC-14 and Palermo red. No cation deficiency at *M*3 was found for the green SGMs in samples IGC-2 and IGC-11, but a deficiency of 12% was obtained in the refinement of the Palermo brown sample, despite there being no partitioning of Zn for this sample. As schoonerite is considered to derive from the Li-containing primary phosphate mineral, triphylite (Moore & Kampf, 1977), the possibility exists that the apparent vacancy at the *M*3 site in SGMs may be explained by Li incorporation at *M*3. Results from LIBS analyses, however, gave only ~0.01 wt% Li in three different schoonerite samples (IGC-11, IGC-14 and IGC-65). This is an order-of-magnitude too low to explain the vacancy concentration.

An interesting observation from inspection of Table 7 is the equivalence of the mean bond lengths for the *M*1 and *M*2 sites and their significant decrease in response to Fe oxidation compared with the *M*3 site. The mean octahedral bond lengths for *M*1 and *M*2 agree to within ≤0.008 Å for all seven recent refinements of SGMs, and both sites undergo a contraction of over 0.1 Å (2.17–2.01 Å) as Fe^{2+} is oxidized to Fe^{3+} in these sites. In contrast, the average *M*3–O bond length remains almost constant over the full range of oxidation, varying only between 2.141 and 2.154 Å. The results reflect a higher susceptibility of Fe to oxidation in the *M*1 and *M*2 sites compared to the *M*3 sites, as indicated by change in the Fe^{2+}/Fe^{3+} contents of the three sites given in Table 6. These results are somewhat puzzling, as *M*1 and *M*2 have quite different coordination environments, $M1O_2(H_2O)_4$ and $M2O_4(OH)_2$, respectively. It might be expected that *M*2 would be more similar to *M*3 in its site chemistry as *M*2 and *M*3 form alternating edge-shared octahedra in the 6.4 Å chains. Indeed, in the closely related mineral flurlite (Grey *et al.*, 2015), a topological isomer of schoonerite, the sites *M*2 and *M*3 become equivalent, with the same coordination.

The close matching of the site occupancies and bond lengths for *M*1 and *M*2 sites in the seven recent refinements is not obeyed by type schoonerite (Kampf, 1977). As seen from Table 7, the mean *M*1−O distance is longer than the mean *M*2−O distance by 0.04 Å in type schoonerite. This difference is significant as the associated standard deviations are 0.007 and 0.004 Å, respectively. A likely explanation for this discrepancy is the incorporation of Ca into the *M*1 site in type schoonerite. Two separate EMP studies on schoonerites from the Palermo No.1 pegmatite (Moore & Kampf, 1977) are consistent in reporting 1.3 and 1.38 wt% CaO, an oxide not present in any of the other schoonerites in Table 7. A plot of Ca *versus* Mn from the EMP analyses shows a negative linear correlation ($R^2 = 0.95$). Substitution of Ca for Mn^{2+} occurs in falsterite (Kampf *et al.*, 2012) and ferraioloite (Mills *et al.*, 2016), as evidenced by the high mean Mn–O distances 2.24–2.27 Å and the low BVS values for Mn^{2+}, 1.58–1.78 Å for these minerals. Both of these minerals have layer structures closely related to that of schoonerite. It is likely that the same substitution occurs in the schoonerite crystal used in the structure refinement by Kampf (1977).

Having established metal atom site occupancies from structure refinements for seven different SGMs from two localities provides an opportunity to look for systematic crystallochemical trends. The results for wilhemgümbelite and schmidite, together with those from the five new refinements are given in Table 6. They show that Zn is consistently dominant in the $^{[5]}$Zn and $^{[4]}$Zn sites, while only Fe^{3+} (plus a trace of Al in schmidite) occupies the *M*4 site. Considerable compositional variation, however, occurs in the *M*1, *M*2 and *M*3 sites. A feature of all samples is the relatively uniform distribution of Mn and Fe across the *M*1, *M*2 and *M*3 sites, whereas excess Zn, beyond that required for the $^{[5]}$Zn/$^{[4]}$Zn sites, tends to order into the *M*3 site. As discussed above, the SGMs show an interesting structural response to increasing oxidation of Fe, whereby Zn in the $^{[5]}$Zn site partially displaces to an adjacent $^{[4]}$Zn site when the fraction of Fe as Fe^{3+} increases above 0.7. There appears to be a correlation between cation deficiency in the *M*3 site and the degree of partitioning of Zn. Taking these factors into consideration a general formula for SGMs can be written as:

$^{[4]}Zn_x\,^{[5]}Zn_{1-x}\,M1\,M2\,(M3_{1-x}\square_x)\,Fe^{3+}(PO_4)_3(OH)_y(H_2O)_{9-y}\cdot 2H_2O$, where □ = vacancy, $x \leq 0.3$ for the known SGMs, and the cations in the *M*1, *M*2 and *M*3 sites are Zn, Mn^{2+}, Fe^{2+} and Fe^{3+}, as well as minor Mg. The value of y is determined by the valence state of Fe and the vacancy concentration; $y = 2$ for schoonerite, which contains only divalent cations, and y increases above 2 with increasing Fe^{3+}.

The different SGMs can be distinguished by the dominant cation occupancy of the *M*1, *M*2 and *M*3 sites and the dominant valency. Wilhelmgümbelite has $M1 = Fe^{3+}$, $M2 = Fe^{3+}$, $M3 = Fe^{2+}$, while schmidite has $M1 = (Fe^{3+}_{0.5}Mn^{2+}_{0.5})$, $M2 = (Fe^{3+}_{0.5}Mn^{2+}_{0.5})$, $M3 = Zn$. That is, in schmidite there are approximately equal amounts of divalent and trivalent cations in both *M*1 and *M*2, where the dominant cations are Mn^{2+} and Fe^{3+}, respectively. The type specimen of schoonerite was reported to have the dominant cation scheme $M1 = Mn^{2+}$, $M2 = Fe^{2+}$, $M3 = Fe^{2+}$ (Kampf, 1977). From the site occupancies in Table 6, the SGM in sample IGC-14 has $M1 = (Fe^{3+}_{0.5}Mn^{2+}_{0.5})$, $M2 = (Fe^{3+}_{0.5}Mn^{2+}_{0.5})$, $M3 = (Mn^{2+}, Zn)$. This represents a new SGM species, and since the completion of this manuscript it has been approved by the IMA CNMNC as a new mineral with the name wildenauerite (Grey *et al.*, 2017d).

The most reduced sample, IGC-11, has Fe^{2+} dominant in all three sites *M*1–*M*3, although it is not clear if this is significant, given the high Mn^{2+} contents and the assumption that the Mn^{2+} is evenly distributed over the three sites. The two Palermo SGMs are difficult to

Downloaded from https://pubs.geoscienceworld.org/eurjmin/article-pdf/30/3/621/4346636/ejm_30_3_0621_0634_grey_2707_online.pdf
by University of Arizona user
on 27 September 2018

categorize, because of co-dominance of different cations in the *M*3 site. Palermo red has clear dominance of $Fe^{3+}>Mn^{2+}$ in *M*1 and *M*2, but *M*3 contains almost equal amounts of Zn, Fe^{2+} and Mn^{2+}. Palermo brown has dominance of $Fe^{2+}>Mn^{2+}$ in *M*1 and *M*2, but with almost equal contents of Zn and Mn^{2+} in *M*3. It is interesting that the SGMs from the Palermo No.1 pegmatite display the same crystallochemical features as those from the Hagendorf Süd pegmatite, despite them having quite different mineral associations and, thus, possibly different parageneses in the two locations. The SGM minerals from both localities have a relatively uniform distribution of Fe, Mn and Zn over the *M*1, *M*2 and *M*3 sites, and display the same partitioning of Zn from the $^{[5]}$Zn site into an adjacent $^{[4]}$Zn site when more than 70% of the Fe is oxidized.

The results presented here illustrate the great difficulty in identifying new occurrences of SGMs. Even when the valence states have been determined for the different cations, and the site occupancies have been established from single-crystal structure refinements, it may still not be possible to assign a particular occurrence to a specific SGM, due to the propensity for uniform cation mixing over the *M* sites.

4. Conclusions

The SGMs from the Hagendorf Süd and Palermo No.1 granitic pegmatites have similar chemistries in relation to the major elements, Fe, Mn and Zn. At both localities, the SGMs are considered to derive from the primary phosphate, triphylite, or its hydrothermal products by reaction with solution zinc from sphalerite alteration.

Zn (at the $^{[5]}$Zn/$^{[4]}$Zn sites) and Fe^{3+} (ordered in the *M*4 site) are essential elements in SGMs. Mn^{2+} and Fe are distributed uniformly over the octahedral sites *M*1, *M*2 and *M*3, with overall Mn/(Mn + Fe) atomic ratios similar to those in the parent triphylite. Manganese is not essential to the schoonerite structure, as evidenced by the low-Mn mineral, wilhelmgümbelite.

The main crystallochemical variations in the samples studied are due to different degrees of oxidation of the Fe, ranging from 45% of the Fe as Fe^{3+} in the green SGM in sample IGC-11, to 97% of Fe as Fe^{3+} in the red SGM in sample IGC-14 (= wildenauerite). The Fe oxidation state is correlated with a significant structural change, whereby Zn in the $^{[5]}$Zn site is partially partitioned into an adjacent $^{[4]}$Zn site when the fraction of Fe as Fe^{3+} increases above 0.7. The Fe oxidation occurs preferentially at the *M*1 and *M*2 sites. Oxidized minerals with $^{[5]}$Zn/$^{[4]}$Zn site partitioning have all iron as Fe^{3+} in the *M*1 and *M*2 sites, whereas the minerals without partitioning have the iron predominantly as Fe^{2+} (>80%) in these two sites. There is an apparent correlation between the extent of partitioning of zinc, and cation deficiency in the *M*3 site. A general formula for SGMs can be written as:

$^{[4]}Zn_x\ ^{[5]}Zn_{1-x}\,M1\,M2\,(M3_{1-x}\square_x)\,Fe^{3+}(PO_4)_3(OH)_y(H_2O)_{9-y}\cdot 2H_2O$, where $\square$ = vacancy, $x \leq 0.3$ for the known SGMs, and the cations in the *M*1, *M*2 and *M*3 sites are Zn, Mn^{2+}, Fe^{2+} and Fe^{3+}, as well as minor Mg. The value of *y* is determined by the valence state of Fe and the vacancy concentration; $y = 2$ for schoonerite, which contains only divalent cations, and *y* increases above 2 with increasing Fe^{3+}. The different SGMs can be distinguished by the dominant cation occupancy of the *M*1, *M*2 and *M*3 sites and the dominant valence state. This has led to the identification and naming of a new SGM, wildenauerite, in specimen IGC-14.

Appendices

A. Verification of valence state of Mn

The reliable determination of site occupancies in SGMs depends on having a knowledge of the valence states of the cations. Fe valence states were determined directly from Mössbauer spectroscopy, or indirectly using the procedure in Appendix B. The Mn valence state was established by combining EMP analyses with mean octahedral *M*−O distances calculated from BV parameters to give weighted *M*−O values averaged over the *M*1–*M*3 sites and equating this to the mean *M*−O for the three sites obtained from the structure refinement. This is illustrated for the example of schmidite, which is the most oxidized SGM mineral and, therefore, the one most likely to have some oxidation of Mn^{2+} to Mn^{3+}.

The empirical cation contents for schmidite in sample IGC-1 from EMP analyses and Mössbauer results are $Zn_{1.47}Mn^{n+}_{0.97}Mg_{0.05}Fe^{2+}_{0.05}Fe^{3+}_{2.26}$, where *n* for Mn is to be determined. From the structure refinement, 1.0 Zn can be assigned to the $^{[5]}$Zn/$^{[4]}$Zn sites, and 1.0 Fe^{3+} to the *M*4 site, giving $Zn_{0.47}Mn^{n+}_{0.97}Mg_{0.05}Fe^{2+}_{0.05}Fe^{3+}_{1.26}$, $\Sigma M = 2.80$, to be assigned to the $M1 + M2 + M3$ sites. The mean *M*−O distances for undistorted octahedra containing these cations can be obtained from their BV parameters (Brown & Altermatt, 1985), giving 2.015, 2.12, 2.12 and 2.14 Å for Fe^{3+}, Mg, Zn and Fe^{2+}, respectively. The weighted octahedral *M*−O distance, averaged over the $M1 + M2 + M3$ sites is then $(1.26 \times 2.015 + 0.52 \times 2.12 + 0.05 \times 2.14 + 0.97 \times Mn^{n+}\text{–O})/2.8$. This can be equated to the experimentally determined mean *M*−O for $M1 + M2 + M3$ sites = 2.113 Å (see Table 7), giving Mn^{n+}–O = 2.235 Å. For comparison the mean Mn^{n+}–O octahedral distances calculated from BV parameters for Mn^{2+} and Mn^{3+} are 2.20 and 2.015 Å, respectively, thus confirming the valence state of Mn as Mn^{2+}. The agreement with Mn^{2+} is improved by correcting for octahedral distortions averaged over the *M*1–*M*3 sites, using the equation relating octahedral bond distance expansion to octahedral distortion developed by Urusov (2003). Applying this correction gives Mn^{n+}–O = 2.22 Å, in closer agreement with Mn^{2+}.

B. Relationship between *a* cell parameter and mean (M1 + M2 + M3)−O bond length

This relationship, illustrated in Fig. 6, was established using EMP analyses together with Mössbauer-determined $Fe^{3+}/(Fe^{2+} + Fe^{3+})$ ratios for seven Hagendorf Süd SGMs. After

Downloaded from https://pubs.geoscienceworld.org/eurjmin/article-pdf/30/3/621/4346636/ejm_30_3_0621_0634_grey_2707_online.pdf
by University of Arizona user
on 27 September 2018

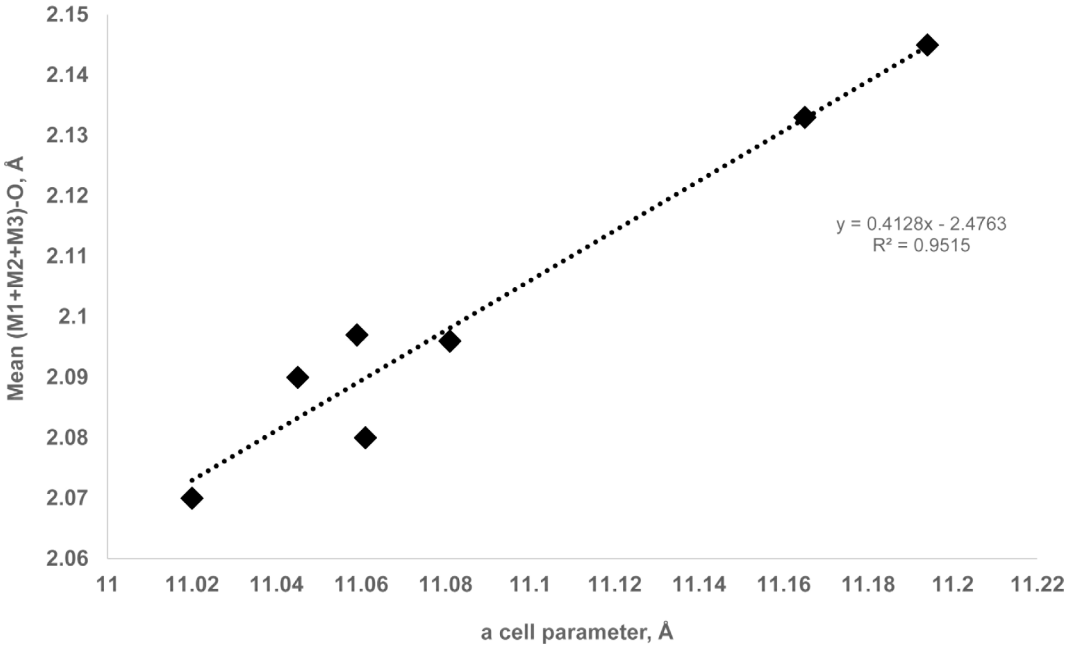

Fig. 6. Relationship between unit-cell parameter a, and the mean metal oxygen distance for $M1 + M2 + M3$ sites.

subtracting 1.0 Zn (in $^{[5]}Zn/^{[4]}Zn$) and 1.0 Fe^{3+} (in $M4$) from the empirical formulae, the remaining cation numbers were used to calculate the mean bond length for the $M1 + M2 + M3$ sites by weighting the bond lengths for individual cations from their BV parameters as described in Appendix A (Mn as Mn^{2+}). The reasonable linear relation obtained between $(M1 + M2 + M3)-O$ and the a cell parameter was used to obtain an estimate of the $Fe^{3+}/(Fe^{2+} + Fe^{3+})$ ratio for the Palermo samples, for which there was too little material to conduct Mössbauer or wet chemical analyses on, but for which total Fe was available from EMP analyses.

Acknowledgements: Thanks to Steve Tassios for the LIBS analyses. A portion of this study was funded by the John Jago Trelawney Endowment to the Mineral Sciences Department of the Natural History Museum of Los Angeles County. The study benefited by access to the microfocus beamline MX2 at the Australian Synchrotron, to collect single-crystal diffraction data.

References

Bosi, F. (2004): Bond valence at mixed occupancy sites − 1. Regular polyhedra. *Acta Crystallogr.*, **B70**, 864–870.

Brown, I.D. & Altermatt, D. (1985): Bond-valence parameters from a systematic analysis of the inorganic crystal structure database. *Acta Crystallogr.*, **B41**, 244–247.

Farrugia, L.J. (1999): WinGX suite for small-molecule single-crystal crystallography. *J. Appl. Crystallogr.*, **32**, 837–838.

Fransolet, A.-M. (2007): Phosphate associations in the granitic pegmatites: the relevant significance of these accessory minerals. Granitic pegmatites: the State of the Art − International Symposium, May 2007. Porto, Portugal.

Grey, I.E., Keck, E., Mumme, W.G., Pring, A. & MacRae, C.M. (2015): Flurlite, $Zn_3Mn^{2+}Fe^{3+}(PO_4)_3(OH)_2 \cdot 9H_2O$, a new mineral from the Hagendorf Süd pegmatite, Bavaria, with a schoonerite-related structure. *Mineral. Mag.*, **79**, 1175−1184.

Grey, I.E., Keck, E., Kampf, A.R., MacRae, C.M., Glenn, A.M. & Price, J.R. (2017a): Wilhelmgümbelite, $[ZnFe^{2+}Fe_3^{3+}(PO_4)_3(OH)_4(H_2O)_5]\cdot 2H_2O$, a new schoonerite-related mineral from the Hagendorf Süd pegmatite, Bavaria. *Mineral. Mag.*, **81**, 287−296.

Grey, I.E., Keck, E., Kampf, A.R., MacRae, C.M., Glenn, A.M., Cashion, J.D. & Gozukara, Y. (2017b): Schmidite, IMA 2017-012. CNMNC Newsletter No. 37, June 2017, page 532. *Eur. J. Mineral.*, **29**, 529−533.

Grey, I.E., Keck, E., Kampf, A.R., MacRae, C.M. & Cashion, J.D. (2017c): A proposal for a schoonerite group and its nomenclature. CNMNC Newsletter No. 40, December 2017, page 1087. *Eur. J. Mineral.*, **29**, 1083–1087.

Grey, I.E., Keck, E., Kampf, A.R., MacRae, C.M., Cashion, J.D., Glenn, A.M., Davidson, C.J. & Gozukara, Y. (2017d): Wildenauerite, IMA 2017-058. CNMNC Newsletter No. 39, October 2017, page 935. *Eur. J. Mineral.*, **29**, 931–936.

Hatert, F. & Burke, E.A.J. (2008): The IMA-CNMNC dominant-constituent rule revisited and extended. *Can. Mineral.*, **46**, 717−728.

Kampf, A.R. (1977): Schoonerite: its atomic arrangement. *Am. Mineral.*, **62**, 250−255.

Kampf, A.R., Mills, S.J., Simmons, W.B., Nizamoff, J.W., Whitmore, R.W. (2012): Falsterite, $Ca_2MgMn^{2+}Fe_2^{2+}Fe_2^{3+}Zn_4(PO_4)_8(OH)_4(H_2O)_{14}$, a new secondary phosphate mineral from the Palermo No.1 pegmatite, North Groton, New Hampshire. *Am. Mineral.*, **97**, 496–502.

Keller, P., Fontan, F. & Fransolet, A.-M. (1994): Intercrystalline partitioning between minerals of the triplite-zwieselite-magniotriplite and the triphylite-lithiophilite series in granitic pegmatites. *Contrib. Mineral. Petrol.*, **118**, 239–248.

Li, Z. & Shinno, I. (1997): Next nearest neighbor in triphylite and related minerals. *Mineral. J.*, **19**, 99–107.

Downloaded from https://pubs.geoscienceworld.org/eurjmin/article-pdf/30/3/621/4346636/ejm_30_3_0621_0634_grey_2707_online.pdf
by University of Arizona user
on 27 September 2018

Mills, S.J., Grey, I.E., Kampf, A.R., MacRae, C.M., Smith, J.B., Davidson, C.J. & Glenn, A.M. (2016): Ferraioloite, $MgMn_4^{2+}(Fe_{0.5}^{2+}Al_{0.5}^{3+})_4Zn_4(PO_4)_8(OH)_4(H_2O)_{20}$, a new secondary phosphate mineral from the Foote mine, USA. *Eur. J. Mineral.*,**28**, 655–661.

Moore, P.B. (1982): Pegmatite minerals of P(V) and B(III). *MAC Short Course Handb.*, **8**, 267–291.

Moore, P.B. (2000): Analyses of primary phosphates from pegmatites in Maine and other localities. in "Mineralogy of Maine. Mining History, Gems, and Geology", V.T. King, ed. Maine Geological Survey, Augusta, Maine, 333–336.

Moore, P.B. & Kampf, A.R. (1977): Schoonerite, a new zinc-manganese-iron phosphate mineral. *Am. Mineral.*, **62**, 246–249.

Mücke, A. (1981): The paragenesis of the phosphate minerals of the Hagendorf pegmatite – a general view. *Chemie der Erde*, **40**, 217–234.

Petříček, V., Dušek, M. & Palatinus, L. (2014): Crystallographic Computing System JANA2006: General features. *Z. Kristallog.*, **229**, 345–352.

Rodriguez-Carvajal, J. (1990): FULLPROF: a program for Rietveld refinement and pattern matching analysis. in: "Proc. of the Satellite Meeting on Powder Diffraction of the XV Congress of the IUCr", Toulouse, France.

Urusov, V.S. (2003): Theoretical analysis and empirical manifestation of the distortion theorem. *Z. Kristallog.*, **218**, 709–719.

Received 24 May 2017
Modified version received 9 October 2017
Accepted 16 October 2017

Downloaded from https://pubs.geoscienceworld.org/eurjmin/article-pdf/30/3/621/4346636/ejm_30_3_0621_0634_grey_2707_online.pdf
by University of Arizona user
on 27 September 2018